Metal Coordination and Enzymatic Reaction of the Glioma-Target R132H Isocitrate Dehydrogenase 1: Insights by Molecular Simulations

Bharath Raghavan,[†,‡] Marco De Vivo,[¶] and Paolo Carloni[*,†,§]

†*Computational Biomedicine, Institute for Neuroscience and Medicine INM-9, Forschungszentrum Jülich GmbH, Jülich 52428, Germany*

‡*Department of Physics, RWTH Aachen University, Aachen 52074, Germany*

¶*Molecular Modelling and Drug Discovery, Italian Institute of Technology, Genova 16163, Italy*

§*Department of Physics and Universitätsklinikum, RWTH Aachen University, Aachen 52074, Germany*

E-mail: p.carloni@fz-juelich.de

Abstract

R132H IDH1 is an important therapeutic target for a variety of brain cancers, yet drug leads and radiotracers which selectively bind only to the mutant over the wild type are so far lacking. Here we have predicted the structural determinants of the Michaelis complex of this mutant using a QM/MM MD-based protocol. It shows some important differences with the X-ray structure, from the metal coordination to the positioning of key residues at the active site. In particular, one lysine residue at the active site emerges as a mostly likely proton donor in the R132H IDH1 catalytic reaction. Intriguingly, the

same residue in its deprotonated state is likely to be involved in the reaction catalyzed by the wild-type enzyme. Our QM/MM protocol could also be used for other metal-based enzymes, which cannot be modelled easily by force field-based MD, like in this case.

Introduction

The NADP-dependent, magnesium-based human Isocitrate Dehydrogenase 1 (IDH1) homodimeric enzyme catalyzes the oxidative decarboxylation of isocitrate (ICT) to α-ketoglutarate (αKG, Equation 1).[1–3]

$$\mathrm{ICT} + \mathrm{NADP}^{+} \longrightarrow \alpha\mathrm{KG} + \mathrm{NADPH} \tag{1}$$

The αKG product regulates the behavior of many dioxygenases enzymes in humans, like the hypoxia-inducible factor-1α and the ten-eleven translocation DNA hydroxylases.[4,5] This has a direct impact on cell stemness and differentiation. Unfortunately, several mutations of this enzyme are involved in a variety of brain cancers. Particularly important is the Arg132His variant (mut-IDH1 hereafter), associated with astrocytoma and oligodendroglioma progression.[6–9]

Mut-IDH1 catalyses the conversion of αKG to 2-hydroxyglutarate (2-HG, Equation 2).[10] 2-HG is a known oncometabolite that promotes stemness in human cells and inhibits DNA demethylases.[11,12]

$$\alpha\mathrm{KG} + \mathrm{NADPH} \longrightarrow 2{-}\mathrm{HG} + \mathrm{NADP}^{+} \tag{2}$$

X-ray studies on the Ca^{2+}-substituted enzyme show that both wt-IDH1[3] and mut-IDH1[10] are dimers (Figure 1A), with each of the two monomers mostly catalytically independent.[13]

The NADP(H) cofactor, the substrate and the metal ion are located in each active sites. The latter include residues from both monomers.[1]

A model of wt-IDH1 Michaelis complex has been obtained from molecular simulation by us and Maria Ramos' group,[14,15] based on the available X-ray structure.[3] Arg100, Arg109, Lys212', Tyr139, Thr75 and Ser94 bind ICT to the active site (Figure 1B). Here, Lys212' (in its deprotonated form) is the most likely residue that initiates the catalysis as a base (Figure 2A).

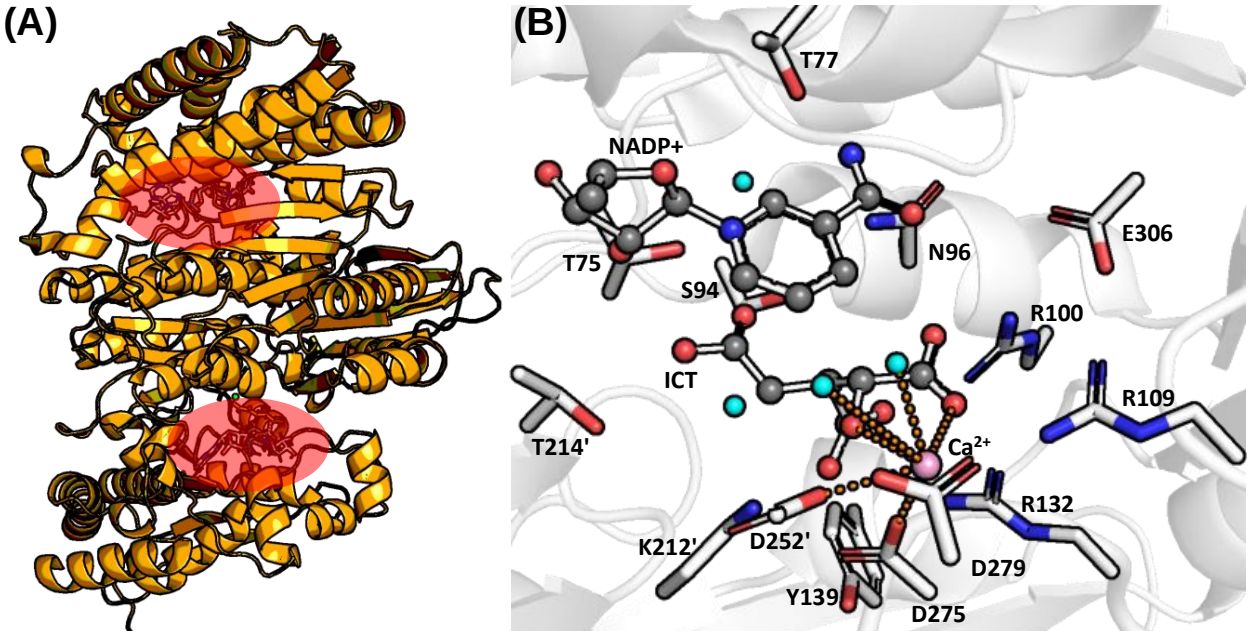

Figure 1: (A) The dimeric structure of IDH1. The two active sites are shown in red. (B) Representation of the wt-IDH1 active site from the X-ray structure. αKG and NADPH are shown in ball-and-sticks representation, while the protein residues are shown as sticks. The Ca^{2+} ion is shown in pink.

For mut-IDH1, indirect information on the Michaelis complex can be obtained by inspection of the X-ray structures (Figure 2B).[10] The Ca^{2+} ion is heptacoordinated. The substrate forms H-bonds with several of the same residues as ICT (Arg100, Arg109, Thr77, Ser94, and Asn96). The mutated residue His132 does not interact with the substrate. Most importantly, the nature of the interaction between αKG and the remaining residues (Lys212', Tyr139 or

[1]In this text, residues from the second subunit are labelled by a dash and those from the first subunit are left unmarked.

Asp275) depend on the protonation states of Lys212' and Asp275. In this text, we refer to the mut-IDH1 protomer with Lys212' deprotonated/Asp275 protonated as $\mathbf{K/D^H}$, and the other way around with $\mathbf{K^H/D}$. We should mention that all X-ray structures of mut-IDH1 (as well as the wild type) complexed with the substrate and cofactor, are catalytically inactive as the Ca^{2+} ion replaces the Mg^{2+} ion.[3,10,16–18] This obviously may lead to a different coordination and hence a different structure of the active site.

The conversion of αKG to 2-HG by mut-IDH1 can also be compared to that of pyruvate to lactate by lactacte dehydrogenase (LDH).[19,20] Both involve reduction of a ketone to alcohol by an acidic residue from the protein, and donation of hydride by nicotinamide ring (NADPH in mut-IDH1 and NADH in LDH). The catalytic mechanism of the enzyme has not been elucidated. One of the major issues is to establish which is the protein residue performing the proton transfer to the α-ketone of αKG (Figure 2C).

Inhibitors which selectively bind mut-IDH1 and not wt-IDH1, so far lacking,[21,22] could be excellent drug leads against glioma. They could also work as positron emission tomography (PET) biomarkers (or radiotracers)[23] for glioma progression by non-invasively and selectively detecting mut-IDH1 expression.[2] Unfortunately, all current proposed ligands do not bind competitively at the substrate site, but rather at the dimer interface.[22,24] This region is structurally similar in both mut- and wt-IDH1, and thus the ligands are not binding-selective.[22]

The drug design efforts for binding-selective inhibitors might greatly profit from the structure of the Michaelis complexes of wt-IDH1 (available from previous QM/MM studies[14,15]) and mut-IDH1 (still lacking). Performing structure-based drug design solely using the inactive crystal structure might lead to incorrect results due to the differences between Ca(II) and Mg(II) coordination chemistry.

[2]PET is a molecular imaging technique which uses specific probes that are labeled with positron-emitting radioisotopes to visualize and measure changes in biological processes in vivo. These probes are referred to as radiotracers, and are labeled with ^{18}F radioactive fluorine isotopes ^{18}F.

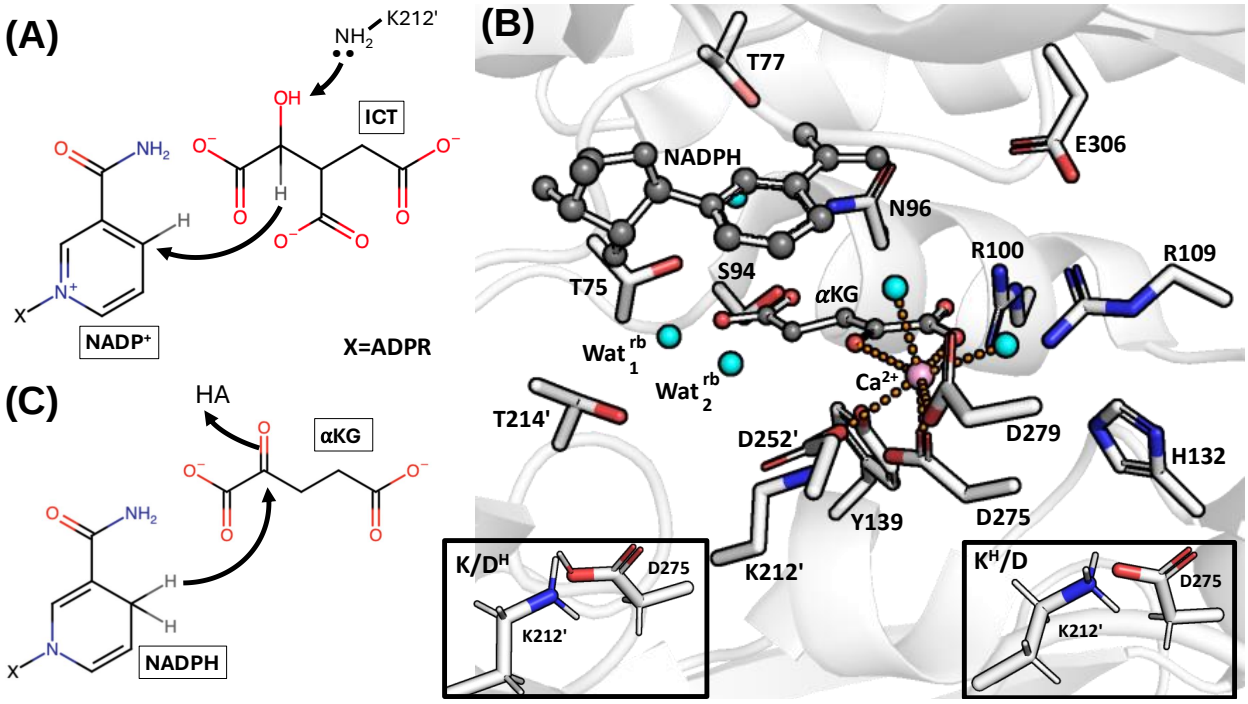

Figure 2: (A) The first step of the oxidative decarboxylation of ICT to αKG as catalysed by wt-IDH1, with Lys212' as the bse initiator.[15] (B) Representation of the mut-IDH1 active site from the X-ray structure. αKG and NADPH are shown in ball-and-sticks representation, while the protein residues are shown as sticks. The Ca^{2+} ion (in pink) binds to the α-carboxylate of αKG, the αKG of ICT, Asp275, Asp252', Asp279 and two water molecules. The nicotinamde group of the NADPH cofactor forms H-bonds Glu306 and Asn96. The ribose alcohol of the cofactor is anchored to αKG by two water molecules, Wat_1^{rb} and Wat_2^{rb}. The former forms H-bonds with the γ-carboxylate of αKG, Wat_2^{rb}, Thr214' and the ribose. Wat_2^{rb} in turn, interacts with the αketone of αKG. Tyr139 H-bonds to Asp275, which in turn forms a salt bridge with Lys212'. Insets of the $\mathbf{K/D^H}$ and $\mathbf{K^H/D}$ protomers are also shown. (C) Proposed reaction mechanism for αKG to 2-HG as catalyzed by mut-IDH1. Here the acid from the protein, HA, is unknown.

Here, based on the X-ray structure of the inactive mut-IDH1/Ca(II) complex (Figure 2B), we have predicted the structural determinants of the active mut-IDH1/Mg(II) complex by using a massively parallel and flexible QM/MM approach developed recently by a large consortium including some of us.[25,26] Simulation of this protein with current classical and QM/MM MD protocols failed (Figure 3A). To obtain the correct coordination sphere of the Mg(II) ion in the active site, a new QM/MM MD protocol was developed (Figure 3B). This involved an initial minimization of the structure at the QM/MM level, and 80 ps of QM/MM dynamics of mut-IDH1. This provides the first insight on active mut-IDH1 for drug design and allows us to suggest that protonated Lys212' is the most likely proton donor in the catalysis.

Methods

General Parameters and Setup

Initial models. We used the human mut-IDH1 enzyme homodimeric X-ray structure, containing two identical active sites features a Ca^{2+} ion, the αKG substrate and the NADPH cofactor (PDB code: 3INM, Figure 2A).[10] First, the Ca^{2+} ion was replaced with a Mg^{2+} ion. Second, we added the N- and C- terminus (Met1 to Lys4 and Ala410 to Leu414), lacking in the X-ray structure, using the Modeller code.[27] Hydrogens were added to the protein using the *pdb2gmx* command in GROMACS.[28] Both the $\mathbf{K/D^H}$ and the $\mathbf{K^H/D}$ protomers were considered (Figure 2B). They were placed in a cubic box of edge length 10.9 nm, and filled with ∼3,800 water molecules, along with 14 sodium ions. The overall systems were neutral.

Force-field based MD setup. The Amber99sb*-ildn force field,[29] TIP3P,[30] and parameters from Ref.[31] were used for the protein, water, and NADPH respectively. The bonded and van der Waals force field parameters for αKG were generated using the Generalised Amber Force Field.[32] The partial charges were calculated using the RESP method at the HF/6-31G* level of theory. This was done using the ANTECHAMBER software package and

ACPYPE.[33,34] NVT MD simulations were achieved using the Nosé-Hoover thermostat[35] at 300 K. NPT MD simulations were achieved using the Parrinello-Rahman barostat[36] at 1 bar with a time constant of 2 ps. Restraints were added by using PLUMED version 2.8.1.[37,38] The GROMACS version 2019.4[39] code was used for all calculations.

QM/MM MD setup. The systems were divided into MM and QM subregions, using the MiMiCPy code.[40] In various step of the MD protocol (discussed later), the following QM subregions were considered (Figure 4A):

Group I consisted of αKG, Mg^{2+}, the nicotinamide ring of NADPH, the water between NADPH ribose and αKG γ-carboxylate, and residues around α-carboxylate of αKG & Mg^{2+} were included: Arg100/109, His132, Tyr139, Lys212', Asp252/275/279, and the two water molecules coordinating with Mg^{2+} (140 QM atoms).

Group II in addition to the previous selection, residues and waters involved in binding to the γ-carboxylate of αKG were included. This consisted of Th77/75/214', Ser94, Asn96. The QM region differed slightly between the $\mathbf{K/D^H}$ and $\mathbf{K^H/D}$ protomers, as some of the residues interacting with αKG differed (179 to 188 QM atoms, details in the SI).

The MM part was described by the same force fields as in the force field-based MD simulations. In the QM region, the quantum problem was solved with density functional theory at the BLYP level.[41] The wavefunction was expanded using a plane-wave basis set up to a cut-off of 100 Ry. The core electrons were described using norm-conserving pseudopotentials.[42] The valence electrons were treated explicitly. The QM region was inserted in a cubic box of edge 2.43 nm. Isolated system conditions were achieved using the Tuckerman method of the Poisson solver.[43]

Open valances at the boundary of the QM-MM covalent bonds were treated with monovalent pseudopotentials.[44] Electrostatic interactions between the QM and MM subsystems were described using the Hamiltonian electrostatic coupling scheme of Laio et. al.[45] The short-

range QM-MM electrostatic interactions were computed explicitly within a cutoff radius of 1.69 nm while the long-range interactions between the point charges of the MM region and the QM charge density were computed using a 5th order multipole expansion of the QM electrostatic potential. QM/MM MD was run using the Born-Oppenheimer approach, with a timestep of 0.5 fs. Temperature was maintained around 300 K using a Nosé-Hoover thermostat. Restraints were added by using PLUMED version 2.8.1, and constraints using the built-in algorithm in CPMD.

The setup and parameters used here are identical to those used by us for simulating the wt-IDH1.[14] All calculations were carried out using GROMACS 2020.3[39] and CPMD 4.3[46] interfaced with MiMiC 0.2.0[47] (including the MiMiC Communication Library 2.0.1[48] for server-client communication).

QM/MM MD Protocol

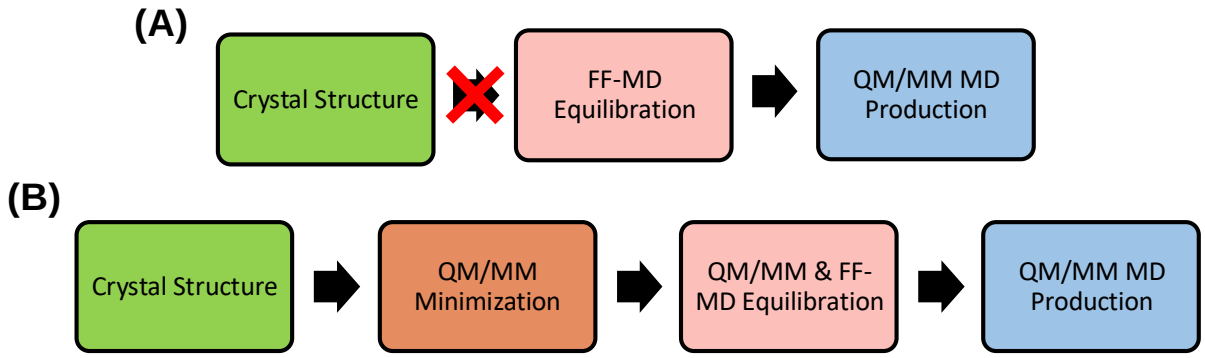

Figure 3: Protocol (A) failed in predicting the Mg^{2+} ion coordination. Hence we used the protocol (B)

MD simulations based on three different force field parameters for Mg^{2+} ions[29,49,50] failed to reproduce the bidentate chelation of αKG with Mg^{2+} (SI). This chelation should be maintained as it plays a crucial role in promoting the catalysis.[10] This points to difficulties that some force fields experience to describe the coordination chemistry of the metal ion in this complex enzyme (Figure 2A). Of course, it is entirely possible that other force fields, not used here, could provide more accurate results. Here, in order to overcome this problem, we

decided to transcend the use of the force fields and use QM/MM simulations. These have shown to accurately reproduce the structural determinants of metalloproteins[51–54] (including wt-IDH1[14]). We utilized the following protocol (Figure 3B):

(1) Energy Minimization.

(A) Steepest descent minimization of the MM hydrogens.

(B) 100 ps of heating from 0 K to 300 K of force-field MD of the water molecules and the sodium ions. The rest of the system was restrained with position restraints on heavy atoms.

(C) 4,000 steps of QM/MM energy-minimization of the entire system. This is done by using simulated annealing, where the temperature is gradually decreased from 300 K to 0 K at a rate of 1% pre timestep. The QM region consisted of **Group I** (Figure 4A), while the remaining atoms were treated at the MM level. The active site of two subunits were alternatively treated at the QM level, while the Mg^{2+} coordination sphere (αKG, Asp252/275/279, and the two water molecules) of the other subunit was kept constrained.

(2) Equilibration.

(A) 2000 steps QM/MM MD heating from 0 to 300 K, followed by ∼8 ps of NVT QM/MM MD. Also here, The QM region consisted of **Group I** (Figure 4A). As in step 1(C), the active sites were alternatively treated at the QM level with the other constrained.

(B) 5 ns NVT and 5 ns NPT force-field based MD, with position restraints on the non-hydrogen atoms.

(C) 500 ns NPT MD without position restraints. Two key interactions at the active site were restrained: (i) the α-ketone of αKG / Mg^{2+} coordination bond (upper wall restraint set at 2.3 Å), (ii) Wat_1^{rb} / NADPH ribose, γ-carboxylate of αKG,

and Thr214' (distance restraints set to ∼1.9 Å).

(3) Production. QM/MM MD of the entire system was performed starting from the last snapshot of step (2)C, using **Group II** as QM region. The two active sites were separately simulated at the QM level by 20 ps QM/MM MD. The other subunit was treated at the MM level with the same restraints as in step (2)C. This was repeated for both Lys212'-H/Asp275 and the Lys212'/Asp275-H protomers, resulting in a total of 80 ps with of QM/MM MD. The last 10 ps for each simulation were used for analysis.

This procedure allowed for the prediction of the Mg^{2+} coordination sphere. In contrast to the force-field based MD, here the metal coordination turned out to be similar to that of the wt-IDH1 (see Results and Discussions).

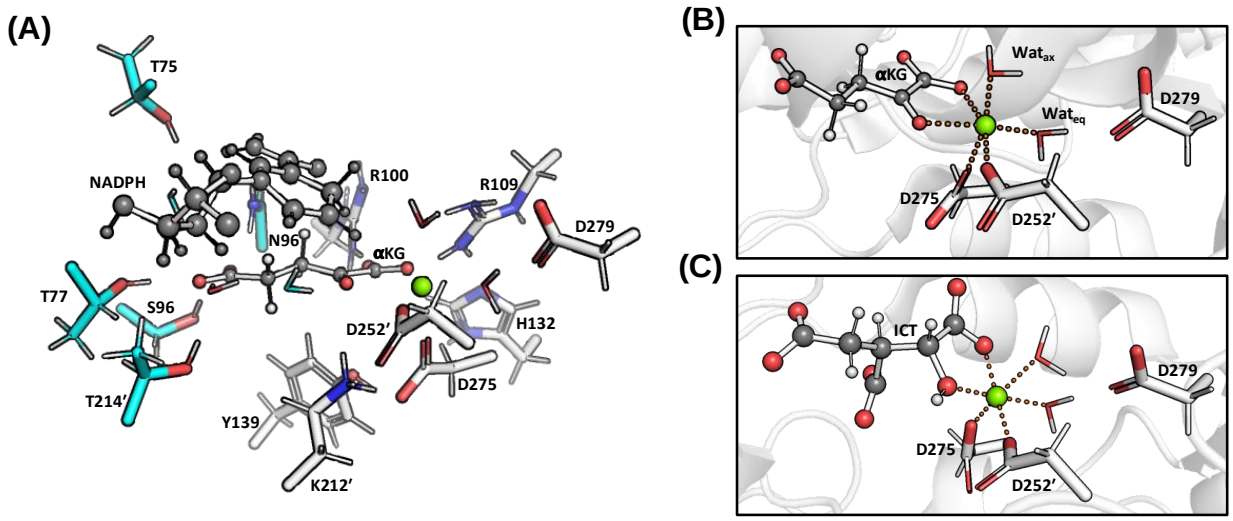

Figure 4: (A) **Group I** (gray) and **Group II** (gray and green) QM regions in the QM/MM calculations. (B) Hexacoordination sphere of Mg^{2+} in the $\mathbf{K^H/D}$ protomer emerging from our QM/MM calculations. The same coordination is also obtained for the $\mathbf{K/D^H}$ protomer. (C) Hexacoordination sphere of Mg^{2+} in wt-IDH1 Michaelis complex obtained from molecular simulation by us.[14]

Results

We used a QM/MM MD protocol (Figure 3B) to predict the structural determinants of both $\mathbf{K/D^H}$ and $\mathbf{K^H/D}$ protomers. Both active sites A and B were simulated alternatively at the

DFT-BLYP QM level, for a total of 80 ps QM/MM MD. Because of the high-scalability of the MiMiC code used for QM/MM simulations,[14,25,55,56] this took only ∼2 weeks on the JUWELS machine in the Juelich Supercomputing System.[57] The deviation of the heavy atoms in the QM region from the X-ray structure at the end of the QM/MM MD is between 1 and 2 Å (SI). Below, we describe our predicted models in detail, starting from a feature which turns out to be the same across all the systems studied: the type of Mg^{2+} ion coordination.

Table 1: Average distance (in Å) from the QM/MM MD simulation of mut-IDH1 between Mg^{2+} and the atoms in its coordination sphere. The α-ketonic oxygen of αKG is not included, as it is given in Table 2.

Protomer	Active Site	αKG α-carboxy	Asp275	Asp252'	Wat_{ax}	Wat_{eq}
$\mathbf{K^H/D}$	A	2.1±0.1	2.0±0.1	2.0±0.1	2.2±0.1	2.1±0.1
	B	2.1±0.1	2.1±0.1	2.1±0.1	2.1±0.1	2.1±0.1
$\mathbf{K/D^H}$	A	2.2±0.1	2.1±0.1	2.1±0.1	2.1±0.1	2.1±0.0
	B	2.2±0.1	2.1±0.1	2.1±0.1	2.2±0.1	2.1±0.1

Mg^{2+} Coordination. In all circumstances, Asp279 does not bind directly to the metal ion as it does to Ca^{2+} in the X-structure. As a result, the Mg(II) ion is hexacoordinated across all of the systems studied here (Figure 4B): namely, this metal ion binds to the α-ketone and α-carboxylate groups of αKG, to the side chains of Asp275 and Asp252', and to equatorial (Wat_{eq}) and axial waters (Wat_{ax}). Wat_{ax} further H-bonds with Asp279. The metal coordination sphere is essentially the same as that in the wt-IDH1/ICT complex, except of course, that the α-alcohol of ICT is replaced by the α-ketone of αKG (Figure 4C). The distances of the coordinating atoms from Mg^{2+} in the metal coordination bonds range between 2.0–2.2 Å (Table 1), except for that between Mg^{2+} and the α-ketonic oxygen. This latter varies with the protomer used, as discussed below.

$\mathbf{K^H/D}$. In both active sites, the α-ketonic oxygen of αKG interact not only with the Mg^{2+} ion, but also forms weak H-bonds to Lys212' and Wat_2^{rb} (Table 2 and Figure 5A). As in the X-ray structure, Wat_2^{rb} forms a H-bond with Wat_1^{rb}, which in turn, interacts with Thr214' and NADPH. Lys212' also forms salt bridges with Asp252' and Asp275. The latter further forms a H-bond with Tyr139. In active site A and the X-ray structure, Arg100/109 bind the

Table 2: Average distance (in Å) from the QM/MM MD simulation of mut-IDH1 between the α-ketonic oxygen of αKG and its interaction partners.

Protomer	Active Site	Mg^{2+}	Lys212'	Wat_{Y139}	Wat_2^{rb}
K^H/D	A	2.4±0.2	2.2±0.2	—	2.5±0.3
	B	2.6±0.2	2.1±0.1	—	2.7±0.6
K/D^H	A	2.3±0.1	—	2.4±0.2	2.7±0.2
	B	2.2±0.1	—	—	2.3±0.2

the α-carboxylate of αKG (as in the X-ray structure), while in active site B this is broken (Figure 5A). Asn96 forms an H-bond with αKG γ-carboxylate active site A (as in the X-ray structure), however this Ans96 moves to bind with the α-carboxylate in active site B.

K/D^H. In both active sites, the α-ketone of αKG binds to the Mg^{2+} ion (Table 2); Lys212' is rotated away from the α-ketone (Figure 5B). It also interacts weakly with Wat_2^{rb}, though this interaction is stronger in active site B. As in the X-ray structure, Wat_2^{rb} forms a H-bond with Wat_1^{rb}, which in turn, interacts with Thr214' and NADPH. Tyr139 establishes a water mediated H-bond with His132 in active site B, and, at times, a water-mediated interaction with the α-ketone of αKG in active site A (Figure 5B and Table 2, where this water is refered to ad Wat_{Y139}; also see SI). Arg100 and Arg109 form H-bonds with α-carboxylate of αKG. Ans96 H-bonds with the γ-carboxylate and forms a water-mediated interaction with NADPH (Figure 5C). The water in the latter interaction is also stabilized by Glu306. These interactions, also present in **K^H/D**, anchor the cofactor to the substrate. Only in active site B of **K^H/D**, is the interaction with Asn96 and γ-carboxylate broken (compare Figures 5A with C).

Discussion

The goal of this work was to obtain the structural determinants of mut-IDH1 Michaelis complex. Attempts to use a variety of force fields (as per the protocol in Figure 3A) did not lead to satisfactory results. We thus used a new QM/MM MD protocol (Figure 3B), which turned out to be more successful.

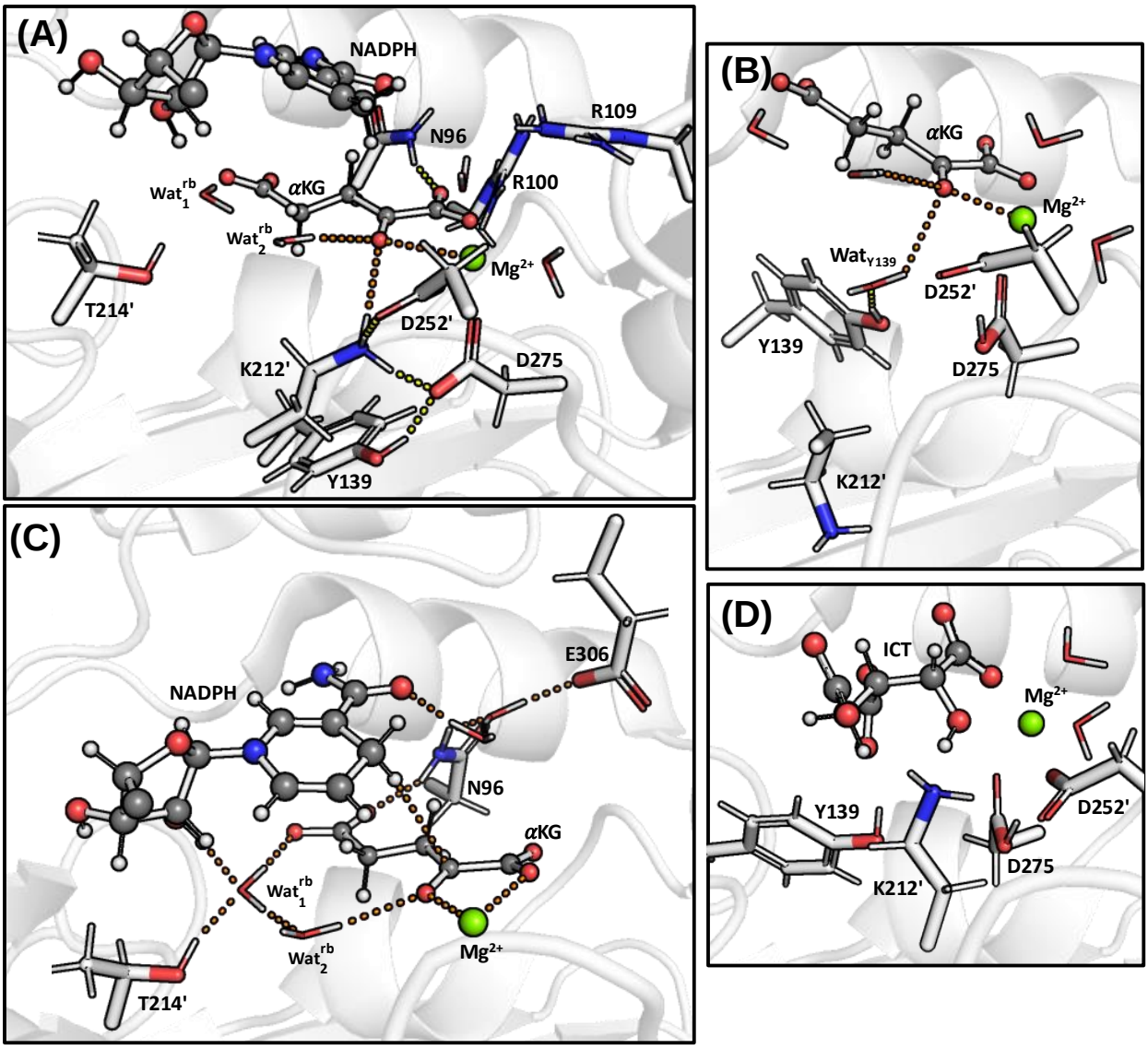

Figure 5: Snapshots of mut-IDH1 after 20 ps of QM/MM MD: (A) Active site B of the $\mathbf{K^H/D}$ protomer showing interactions of the α-ketone of αKG (in orange), and those of Lys212', Tyr139, and Asn96. (B) Active site A of the $\mathbf{K/D^H}$ protomer showing interactions of the α-ketone of αKG (in orange), especially with $\mathrm{Wat_{Y139}}$. (C) Active site B of the $\mathbf{K/D^H}$ protomer showing the interactions that anchor NADPH close to αKG (in orange). (D) Snapshot of ICT–Lys212' (deprotonated) in the wt-IDH1 active site from Ref.[15]

Our calculations suggest that, irrespective of the protonation state of Lys212' and Asp275, the metal ion is hexacoordinated. The ion binds to Asp275/252', two water molecules, and to the substrate (Figure 4B). This contrasts with the Ca^{2+} in the X-ray structure, which is heptacoordinated (Figure 2B). This is likely one important reason why the enzyme is inactivated by Ca^{2+} ions. The magnesium coordination sphere in the αKG/mut-IDH1 complex is similar to that of the ICT/wt-IDH1 complex (Figure 4C), except that the substrate-Mg^{2+} binding in wt-IDH1 is much stronger. The αKG–Mg^{2+} binding distance, especially in $\mathbf{K^H/D}$, is more elongated than the expected distance of 2.1 Å (Table 2). This is likely due to the extra proton on Lys212' pulling the α-ketone of αKG away from the Mg^{2+} coordination sphere. Our result is thus consistent with the claim by a previous study that states that the αKG–Mg^{2+} binding in mut-IDH1 is weaker than the ICT-Mg^{2+} binding in wt-IDH1.[58] Such a weak interaction between αKG and Mg^{2+} may be difficult to describe by standard force fields (as suggested by our own work here), which, in the way they are built, may assume an ideal octahedral geometry.

A second difference with the X-ray structure[10] is the location of residues which can act as proton donor to the α-ketone of αKG in the enzymatic reaction (Figure 5A). Inspection of the catalytically inactive X-ray structure show that Lys212', Asp275 and Tyr139 interact with the ketone moiety of the substrate. However according to our calculations, Lys212' in its positively charged (protonated) state is the most likely residue to protonate the substrate, as it is the only one forming an H-bond with the α-ketone in the QM/MM Michaelis complex. The other two are at least as far as 4 Å from the α-ketone of αKG (Figure 5B and SI for more details). This finding is consistent with mutagensis experiments, which show that Y139D-IDH1 is still able to catalyze the reaction.[16] Interestingly, Lys212' (in its deprotonated state) is involved in the deprotonation of the substrate (ICT) in the wt-IDH1.[14,15] Thus, the same residue appears to be well positioned to perform proton transfers in both wt- and mut-IDH1 isoforms (compare the position of Lys212' vis á vis the substrate in Figures 5A and D).

Conclusions

Developing binders selective to mut-IDH1 over wt-IDH1 could have wide-ranging applications, from PET radiotracers for early, non-invasive diagnosis of IDH1-associated glioma to anti-brain cancer drugs. Together with our previous work, we have provided the structural determinants of wt- and mut-IDH1. The latter structure show crucial differences with the X-ray structure, from the metal coordination to the positioning of key residues at the active site. In particular, our predictions further allow us to suggest that Lys212' is the mostly likely proton donor in the mut-IDH1 catalytic reaction. The same residue (deprotonated) is also important in the wt-IDH1 catalysis as a proton acceptor. Thus, it appears that Lys212' performs the required proton transfers in both wt- and mut-IDH1 isoforms. Importantly, our structures may be used as templates for the design of binding-selective ligands, which unfortunately have not been identified yet.

The structures will be made publicly available when this work is published in a peer-reviewed journal. Our group is currently working to utilize these structures in a drug design protocol for suggesting radiotracer precursor candidates of mut-IDH1.

Acknowledgement

BR, MDV, PC thank the Helmholtz European Partnering program ("Innovative high-performance computing approaches for molecular neuromedicine") for funding. PC thanks the Human Brain Project (EU Horizon 2020) for funding. BR and PC acknowledge the Gauss Centre for Supercomputing e.V. (www.gauss-centre.eu) for funding this project by providing computing time through the John von Neumann Institute for Computing (NIC) on the GCS Supercomputer JUWELS[57] at Jülich Supercomputing Centre (JSC). BR also gratefully acknowledges discussions with Emiliano Ippoliti, Davide Mandelli and Florian K. Schackert.

Supporting Information Available

Supporting Information Available: description of the unconstrained classical MD simulations that failed in simulating mut-IDH1; snapshots of the exact QM region used the QM/MM MD simulations; an analysis on the interaction between αKG and Tyr139/Asp275. (PDF)

References

(1) Gonçalves, S.; Miller, S. P.; Carrondo, M. A.; Dean, A. M.; Matias, P. M. Induced fit and the catalytic mechanism of isocitrate dehydrogenase. *Biochemistry* **2012**, *51*, 7098–7115.

(2) Quartararo, C. E.; Hazra, S.; Hadi, T.; Blanchard, J. S. Structural, kinetic and chemical mechanism of isocitrate dehydrogenase-1 from mycobacterium tuberculosis. *Biochemistry* **2013**, *52*, 1765–1775.

(3) Xu, X.; Zhao, J.; Xu, Z.; Peng, B.; Huang, Q.; Arnold, E.; Ding, J. Structures of human cytosolic NADP-dependent isocitrate dehydrogenase reveal a novel self-regulatory mechanism of activity. *The Journal of biological chemistry* **2004**, *279*, 33946–33957.

(4) Tennant, D. A.; Frezza, C.; MacKenzie, E. D.; Nguyen, Q. D.; Zheng, L.; Selak, M. A.; Roberts, D. L.; Dive, C.; Watson, D. G.; Aboagye, E. O.; Gottlieb, E. Reactivating HIF prolyl hydroxylases under hypoxia results in metabolic catastrophe and cell death. *Oncogene 2009 28:45* **2009**, *28*, 4009–4021.

(5) Carey, B. W.; Finley, L. W.; Cross, J. R.; Allis, C. D.; Thompson, C. B. Intracellular α-ketoglutarate maintains the pluripotency of embryonic stem cells. *Nature 2014 518:7539* **2014**, *518*, 413–416.

(6) Weller, M. et al. EANO guidelines on the diagnosis and treatment of diffuse gliomas of adulthood. *Nature Reviews Clinical Oncology 2020 18:3* **2020**, *18*, 170–186.

(7) Louis, D. N.; Perry, A.; Wesseling, P.; Brat, D. J.; Cree, I. A.; Figarella-Branger, D.; Hawkins, C.; Ng, H. K.; Pfister, S. M.; Reifenberger, G.; Soffietti, R.; Von Deimling, A.; Ellison, D. W. The 2021 WHO Classification of Tumors of the Central Nervous System: a summary. *Neuro-Oncology* **2021**, *23*, 1231.

(8) Horbinski, C. What do we know about IDH1/2 mutations so far, and how do we use it? *Acta neuropathologica* **2013**, *125*, 621–636.

(9) Huang, L. E. Friend or foe—IDH1 mutations in glioma 10 years on. *Carcinogenesis* **2019**, *40*, 1299–1307.

(10) Dang, L. et al. Cancer-associated IDH1 mutations produce 2-hydroxyglutarate. *Nature* **2009**, *462*, 739–744.

(11) Wu, H.; Zhang, Y. Reversing DNA methylation: mechanisms, genomics, and biological functions. *Cell* **2014**, *156*, 45–68.

(12) Guo, J. U.; Su, Y.; Zhong, C.; Ming, G. L.; Song, H. Hydroxylation of 5-methylcytosine by TET1 promotes active DNA demethylation in the adult brain. *Cell* **2011**, *145*, 423–434.

(13) Pietrak, B.; Zhao, H.; Qi, H.; Quinn, C.; Gao, E.; Boyer, J. G.; Concha, N.; Brown, K.; Duraiswami, C.; Wooster, R.; Sweitzer, S.; Schwartz, B. A tale of two subunits: How the neomorphic R132H IDH1 mutation enhances production of αHG. *Biochemistry* **2011**, *50*, 4804–4812.

(14) Raghavan, B.; Paulikat, M.; Ahmad, K.; Callea, L.; Rizzi, A.; Ippoliti, E.; Mandelli, D.; Bonati, L.; De Vivo, M.; Carloni, P. Drug Design in the Exascale Era: A Perspective from Massively Parallel QM/MM Simulations. *Journal of Chemical Information and Modeling* **2023**, *63*, 3647–3658.

(15) Neves, R. P.; Fernandes, P. A.; Ramos, M. J. Unveiling the Catalytic Mechanism of NADP+-Dependent Isocitrate Dehydrogenase with QM/MM Calculations. *ACS Catalysis* **2016**, *6*, 357–368.

(16) Rendina, A. R.; Pietrak, B.; Smallwood, A.; Zhao, H.; Qi, H.; Quinn, C.; Adams, N. D.; Concha, N.; Duraiswami, C.; Thrall, S. H.; Sweitzer, S.; Schwartz, B. Mutant IDH1 Enhances the Production of 2-Hydroxyglutarate Due to Its Kinetic Mechanism. *Biochemistry* **2013**, *52*, 4563–4577.

(17) Reinbold, R.; Hvinden, I. C.; Rabe, P.; Herold, R. A.; Finch, A.; Wood, J.; Morgan, M.; Staudt, M.; Clifton, I. J.; Armstrong, F. A.; McCullagh, J. S.; Redmond, J.; Bardella, C.; Abboud, M. I.; Schofield, C. J. Resistance to the isocitrate dehydrogenase 1 mutant inhibitor ivosidenib can be overcome by alternative dimer-interface binding inhibitors. *Nature Communications 2022 13:1* **2022**, *13*, 1–12.

(18) Liu, X.; Reinbold, R.; Liu, S.; Herold, R. A.; Rabe, P.; Duclos, S.; Yadav, R. B.; Abboud, M. I.; Thieffine, S.; Armstrong, F. A.; Brewitz, L.; Schofield, C. J. Natural and synthetic 2-oxoglutarate derivatives are substrates for oncogenic variants of human isocitrate dehydrogenase 1 and 2. *Journal of Biological Chemistry* **2023**, *299*, 102873–102874.

(19) widerek, K.; Tuñón, I.; Martí, S.; Moliner, V. Protein conformational landscapes and catalysis. Influence of active site conformations in the reaction catalyzed by L-lactate dehydrogenase. *ACS Catalysis* **2015**, *5*, 1172–1185.

(20) Peng, H.-L.; Deng, H.; Dyer, R. B.; Callender, R. Energy Landscape of the Michaelis Complex of Lactate Dehydrogenase: Relationship to Catalytic Mechanism. *Biochemistry* **2014**, *53*, 1849–1857.

(21) Chitneni, S. K.; Reitman, Z. J.; Spicehandler, R.; Gooden, D. M.; Yan, H.; Zalutsky, M. R. Synthesis and evaluation of radiolabeled AGI-5198 analogues as candidate

radiotracers for imaging mutant IDH1 expression in tumors. *Bioorganic & Medicinal Chemistry Letters* **2018**, *28*, 694–699.

(22) Liu, S.; Abboud, M.; Mikhailov, V.; Liu, X.; Reinbold, R.; Schofield, C. J. Differentiating Inhibition Selectivity and Binding Affinity of Isocitrate Dehydrogenase 1 Variant Inhibitors. *Journal of Medicinal Chemistry* **2023**, *66*, 5279–5288.

(23) Chitneni, S. K. IDH1 Mutations in Glioma: Considerations for Radiotracer Development. *SM radiology journal* **2016**, *2*.

(24) Deng, G. et al. Selective inhibition of mutant isocitrate dehydrogenase 1 (IDH1) via disruption of a metal binding network by an allosteric small molecule. *Journal of Biological Chemistry* **2015**, *290*, 762–774.

(25) Olsen, J. M. H.; Bolnykh, V.; Meloni, S.; Ippoliti, E.; Bircher, M. P.; Carloni, P.; Rothlisberger, U. MiMiC: A Novel Framework for Multiscale Modeling in Computational Chemistry. *Journal of Chemical Theory and Computation* **2019**, *15*, 3810–3823.

(26) Antalík, A. et al. MiMiC: A high-performance framework for multiscale molecular dynamics simulations. *Journal of Chemical Physics* **2024**, *161*.

(27) Šali, A.; Blundell, T. L. Comparative protein modelling by satisfaction of spatial restraints. *Journal of molecular biology* **1993**, *234*, 779–815.

(28) Van Der Spoel, D.; Lindahl, E.; Hess, B.; Groenhof, G.; Mark, A. E.; Berendsen, H. J. GROMACS: fast, flexible, and free. *Journal of computational chemistry* **2005**, *26*, 1701–1718.

(29) Hornak, V.; Abel, R.; Okur, A.; Strockbine, B.; Roitberg, A.; Simmerling, C. Comparison of multiple Amber force fields and development of improved protein backbone parameters. *Proteins* **2006**, *65*, 712–725.

(30) Mark, P.; Nilsson, L. Structure and dynamics of the TIP3P, SPC, and SPC/E water models at 298 K. *Journal of Physical Chemistry A* **2001**, *105*.

(31) Holmberg, N.; Ryde, U.; Bülow, L. Redesign of the coenzyme specificity in l-Lactate dehydrogenase from Bacillus stearothermophilus using site-directed mutagenesis and media engineering. *Protein Engineering, Design and Selection* **1999**, *12*, 851–856.

(32) Wang, J.; Wolf, R. M.; Caldwell, J. W.; Kollman, P. A.; Case, D. A. Development and testing of a general amber force field. *Journal of Computational Chemistry* **2004**, *25*, 1157–1174.

(33) Sousa Da Silva, A. W.; Vranken, W. F. ACPYPE - AnteChamber PYthon Parser interfacE. *BMC Research Notes* **2012**, *5*, 1–8.

(34) Wang, J.; Wang, W.; Kollman, P. A.; Case, D. A. Automatic atom type and bond type perception in molecular mechanical calculations. *Journal of Molecular Graphics and Modelling* **2006**, *25*, 247–260.

(35) Nosé, S. A unified formulation of the constant temperature molecular dynamics methods. *The Journal of Chemical Physics* **1998**, *81*, 511.

(36) Parrinello, M.; Rahman, A. Crystal Structure and Pair Potentials: A Molecular-Dynamics Study. *Physical Review Letters* **1980**, *45*, 1196.

(37) Bonomi, M. et al. Promoting transparency and reproducibility in enhanced molecular simulations. *Nature Methods 2019 16:8* **2019**, *16*, 670–673.

(38) Tribello, G. A.; Bonomi, M.; Branduardi, D.; Camilloni, C.; Bussi, G. PLUMED 2: New feathers for an old bird. *Computer Physics Communications* **2014**, *185*, 604–613.

(39) Abraham, M. J.; Murtola, T.; Schulz, R.; Páll, S.; Smith, J. C.; Hess, B.; Lindah, E. GROMACS: High performance molecular simulations through multi-level parallelism from laptops to supercomputers. *SoftwareX* **2015**, *1-2*, 19–25.

(40) Raghavan, B.; Schackert, F. K.; Levy, A.; Johnson, S. K.; Ippoliti, E.; Mandelli, D.; Olsen, J. M. H.; Rothlisberger, U.; Carloni, P. MiMiCPy: An Efficient Toolkit for MiMiC-Based QM/MM Simulations. *Journal of Chemical Information and Modeling* **2023**, *63*, 1406–1412.

(41) Becke, A. D. Density-functional thermochemistry. I. The effect of the exchange-only gradient correction. *The Journal of Chemical Physics* **1992**, *96*, 2155–2160.

(42) Troullier, N.; Martins, J. L. Efficient pseudopotentials for plane-wave calculations. *Physical Review B* **1991**, *43*, 1993–2006.

(43) Martyna, G. J.; Tuckerman, M. E. A reciprocal space based method for treating long range interactions in ab initio and force-field-based calculations in clusters. *The Journal of Chemical Physics* **1999**, *110*, 2810–2821.

(44) Von Lilienfeld, O. A.; Tavernelli, I.; Rothlisberger, U.; Sebastiani, D. Variational optimization of effective atom centered potentials for molecular properties. *The Journal of Chemical Physics* **2004**, *122*, 014113.

(45) Laio, A.; VandeVondele, J.; Rothlisberger, U. A Hamiltonian electrostatic coupling scheme for hybrid Car–Parrinello molecular dynamics simulations. *The Journal of Chemical Physics* **2002**, *116*, 6941.

(46) Hutter, J.; Alavi, A.; Deutsch, T.; Bernasconi, M.; Goedecker, S.; Marx, D.; Tuckerman, M.; Parrinello, M. CPMD, Copyright IBM Corp 1990-2022, Copyright MPI für Festkörperforschung Stuttgart 1997-2001. `http://www.cpmd.org/`.

(47) Olsen, J. M. H.; Bolnykh, V.; Meloni, S.; Ippoliti, E.; Carloni, P.; Rothlisberger, U. MiMiC: A Framework for Multiscale Modeling in Computational Chemistry (v0.2.0). 2022.

(48) Bolnykh, V.; Olsen, J. M. H.; Meloni, S.; Ippoliti, E.; Carloni, P.; Rothlisberger, U. MiMiC Communication Library (v2.0.1). 2022.

(49) Zhang, Y.; Jiang, Y.; Peng, J.; Zhang, H. Rational Design of Nonbonded Point Charge Models for Divalent Metal Cations with Lennard-Jones 12-6 Potential. *Journal of Chemical Information and Modeling* **2021**, *61*, 4031–4044.

(50) Grotz, K. K.; Cruz-León, S.; Schwierz, N. Optimized Magnesium Force Field Parameters for Biomolecular Simulations with Accurate Solvation, Ion-Binding, and Water-Exchange Properties. *Journal of Chemical Theory and Computation* **2021**, *17*, 2530–2540.

(51) Lukoyanov, D. A.; Yang, Z.-Y.; Dean, D. R.; Seefeldt, L. C.; Raugei, S.; Hoffman, B. M. Electron Redistribution within the Nitrogenase Active Site FeMo-Cofactor During Reductive Elimination of H ¡sub¿2¡/sub¿ to Achieve NN Triple-Bond Activation. *Journal of the American Chemical Society* **2020**, *142*, 21679–21690.

(52) Calandrini, V.; Rossetti, G.; Arnesano, F.; Natile, G.; Carloni, P. Computational metallomics of the anticancer drug cisplatin. *Journal of Inorganic Biochemistry* **2015**, *153*, 231–238.

(53) Ho, M. H.; De Vivo, M.; Peraro, M. D.; Klein, M. L. Unraveling the catalytic pathway of metalloenzyme farnesyltransferase through QM/MM computation. *Journal of Chemical Theory and Computation* **2009**, *5*, 1657–1666.

(54) Wu, R.; Hu, P.; Wang, S.; Cao, Z.; Zhang, Y. Flexibility of catalytic zinc coordination in thermolysin and HDAC8: A Born-Oppenheimer ab initio QM/MM molecular dynamics study. *Journal of Chemical Theory and Computation* **2010**, *6*, 337–343.

(55) Chiariello, M. G.; Bolnykh, V.; Ippoliti, E.; Meloni, S.; Olsen, J. M. H.; Beck, T.; Rothlisberger, U.; Fahlke, C.; Carloni, P. Molecular Basis of CLC Antiporter Inhibition by Fluoride. *Journal of the American Chemical Society* **2020**, *142*, 7254–7258.

(56) Chiariello, M. G.; Alfonso-Prieto, M.; Ippoliti, E.; Fahlke, C.; Carloni, P. Mechanisms Underlying Proton Release in CLC-type F-/H+Antiporters. *Journal of Physical Chemistry Letters* **2021**, *12*, 4415–4420.

(57) Alvarez, D. JUWELS Cluster and Booster: Exascale Pathfinder with Modular Supercomputing Architecture at Juelich Supercomputing Centre. *Journal of large-scale research facilities JLSRF* **2021**, *7*, A183.

(58) Liu, S.; Abboud, M. I.; John, T.; Mikhailov, V.; Hvinden, I.; Walsby-Tickle, J.; Liu, X.; Pettinati, I.; Cadoux-Hudson, T.; McCullagh, J. S.; Schofield, C. J. Roles of metal ions in the selective inhibition of oncogenic variants of isocitrate dehydrogenase 1. *Communications Biology 2021 4:1* **2021**, *4*, 1–16.